Neuronal morphology and physiology, functional brain networks and memory in temporal lobe epilepsy

Linda Douw[1,2], Ida A. Nissen[3], Sophie M.D.D. Fitzsimmons[1], Arjan Hillebrand[3], Elisabeth C.W. van Straaten[3], Cornelis J. Stam[3], Philip C. De Witt Hamer[4], Johannes C. Baayen[4], Martin Klein[5], Jaap C. Reijneveld[6,7], Djai B. Heyer[8], Matthijs B. Verhoog[8,9], René Wilbers[8], Sarah Hunt[8], Huibert D. Mansvelder[8], Jeroen J.G. Geurts[1], Christiaan P.J. de Kock*[8], Natalia A. Goriounova*[8]

* contributed equally

Affiliations

1 Department of Anatomy and Neurosciences, Amsterdam UMC, Vrije Universiteit Amsterdam, Amsterdam Neuroscience, the Netherlands

2 Department of Radiology, Athinoula A. Martinos Center for Biomedical Imaging, Massachusetts General Hospital, USA

3 Department of Clinical Neurophysiology and MEG Center, Amsterdam UMC, Vrije Universiteit Amsterdam, Amsterdam Neuroscience, the Netherlands

4 Department of Neurosurgery, Amsterdam UMC, Vrije Universiteit Amsterdam, Amsterdam Neuroscience, VUmc Cancer Center Amsterdam Brain Tumor Center Amsterdam, the Netherlands

5 Department of Medical Psychology, Amsterdam UMC, Vrije Universiteit Amsterdam, Amsterdam Neuroscience, VUmc Cancer Center Amsterdam Brain Tumor Center Amsterdam, the Netherlands

6 Department of Neurology, Amsterdam UMC, Vrije Universiteit Amsterdam, Amsterdam Neuroscience, VUmc Cancer Center Amsterdam Brain Tumor Center Amsterdam, the Netherlands

7 Stichting Epilepsie Instellingen Nederland (SEIN), Heemstede, the Netherlands

8 Department of Integrative Neurophysiology, Center for Neurogenomics and Cognitive Research (CNCR), Vrije Universiteit Amsterdam, Amsterdam Neuroscience, the Netherlands

9 Department of Human Biology, Division of Cell Biology, Neuroscience Institute, University of Cape Town, South Africa

ABSTRACT

Temporal lobe epilepsy patients are heterogeneous regarding cognitive functioning, with predominant risk of memory deficits. Despite major advances within cellular neuroscience, neuroimaging, and neuropsychology, it remains challenging to integrate memory performance with cellular characteristics and brain network topology. In a unique dataset, we investigate these cross-scale individual differences. Preoperatively, drug-resistant temporal lobe epilepsy patients (*n* = 31, 15 females) underwent functional magnetic resonance imaging, magnetoencephalography and/or memory testing. Macro-scale network centrality was determined, since this number of integrative functional connections a region has is crucial for memory functioning. Subsequently, non-pathological cortical tissue resected from the lateral middle temporal gyrus (default mode network) was used for single cell morphological (total dendritic length) and electrophysiological patch-clamp analysis (action potential rise speed). We expected greater macro-scale centrality to relate to longer micro-scale dendritic length and faster action potentials, and greater centrality to relate to better memory performance. Greater macro-scale centrality correlated with longer dendritic length and faster action potentials (canonical

correlation coefficient = 0.329, $p < 0.001$). Moreover, greater macro-scale centrality was related to better memory performance (canonical correlation coefficient = 0.234, $p = 0.013$). We conclude that more complex neuronal morphology and faster action potential kinetics are mirrored by more integrative functional network topology of the middle temporal gyrus, which in turn is associated with better memory functioning. Thus, our cross-scale analyses reveal a significant relationship between cellular and imaging measures of network topology in the brain, which support cognitive performance in these patients.

Introduction

A long-standing question in clinical neuroscience is how to integrate vastly different scales of investigation to better understand the brain. Cross-scale analysis of neural organizational principles in the same individual is typically difficult: mechanistic work is performed at the level of individual neurons in animals or postmortem samples, while clinical research takes place at the level of behavioral testing and macro-scale neuroimaging, leaving a wide translational gap between the two. In patients with temporal lobe epilepsy (TLE), both scales of investigation have been exploited: a subgroup of patients undergoes craniotomy to resect the presumed seizure origin, allowing for histopathological work that has given major insights into disease pathophysiology [1]. Patients also undergo an extensive clinical work-up before surgery, including imaging, neurophysiological recording and cognitive testing [2,3]. However, an understanding of often-reported and clinically relevant individual differences across scales is lacking.

Recent macro-scale investigations suggest that cognition may be explained by whole-brain structural connections between brain areas, and the orchestrated functional dynamics taking place on top of that structural network [4,5]. Network neuroscience allows for characterization of this network, consisting of nodes (brain regions) and edges between them (structural or functional connections). While structural connections are usually determined using diffusion magnetic resonance imaging (dMRI), functional connections can be estimated using resting-state functional MRI (rsfMRI) or magnetoencephalography (MEG), assessing different aspects of synchronized brain activity. Despite using different modalities, functional network topology has consistently been shown to be relevant for cognitive capabilities in healthy persons [6], in patients suffering from neurological disease [4] and in TLE patients specifically [7,8]. An open question is

whether combining different imaging and neurophysiological modalities may improve explanation of cognitive variance in these patients. Multilayer network theory provides a framework to integrate such modalities into a single network consisting of interconnected layers [9]. Previous work suggests that multilayer functional brain network properties supersede unilayer network characteristics in explaining cognitive functioning in Alzheimer's disease patients [10].

The most important properties of brain networks in relation to cognition are segregation and integration [11–13]. Segregation refers to the extent to which nodes are locally interconnected, and integration signifies the level of integrative connectivity taking place, either in globally or at a particular node. At specific brain regions, the extent of segregation and integration typically show opposite patterns [14,15]: certain regions have a more segregative topological role (e.g. regions within the visual system), while others are considered mainly integrative (e.g. regions in the frontal lobe), indicating that brain regions tend to have a 'typical' role in the brain network that can be quantified with either segragative or integrative network measures. For example, centrality indicates the expected level of network integration occurring at any particular node (see figure 1B on the next page), with nodes showing high integration most likely having low segregation.

Cognitively impaired TLE patients, with pathology of and around the hippocampus, predominantly suffer from memory dysfunction [16]. Integrative connectivity of the temporal lobe, also overlapping with the default mode network (DMN [17]), may be paramount to explain individual memory differences [18–20]. An exemplar study explored the integrative connectivity

of the hippocampal circuit with the posterior DMN [21], reporting that greater memory deficits were related to lower network integration.

Figure 1. Schematic representation of multi-scale analyses

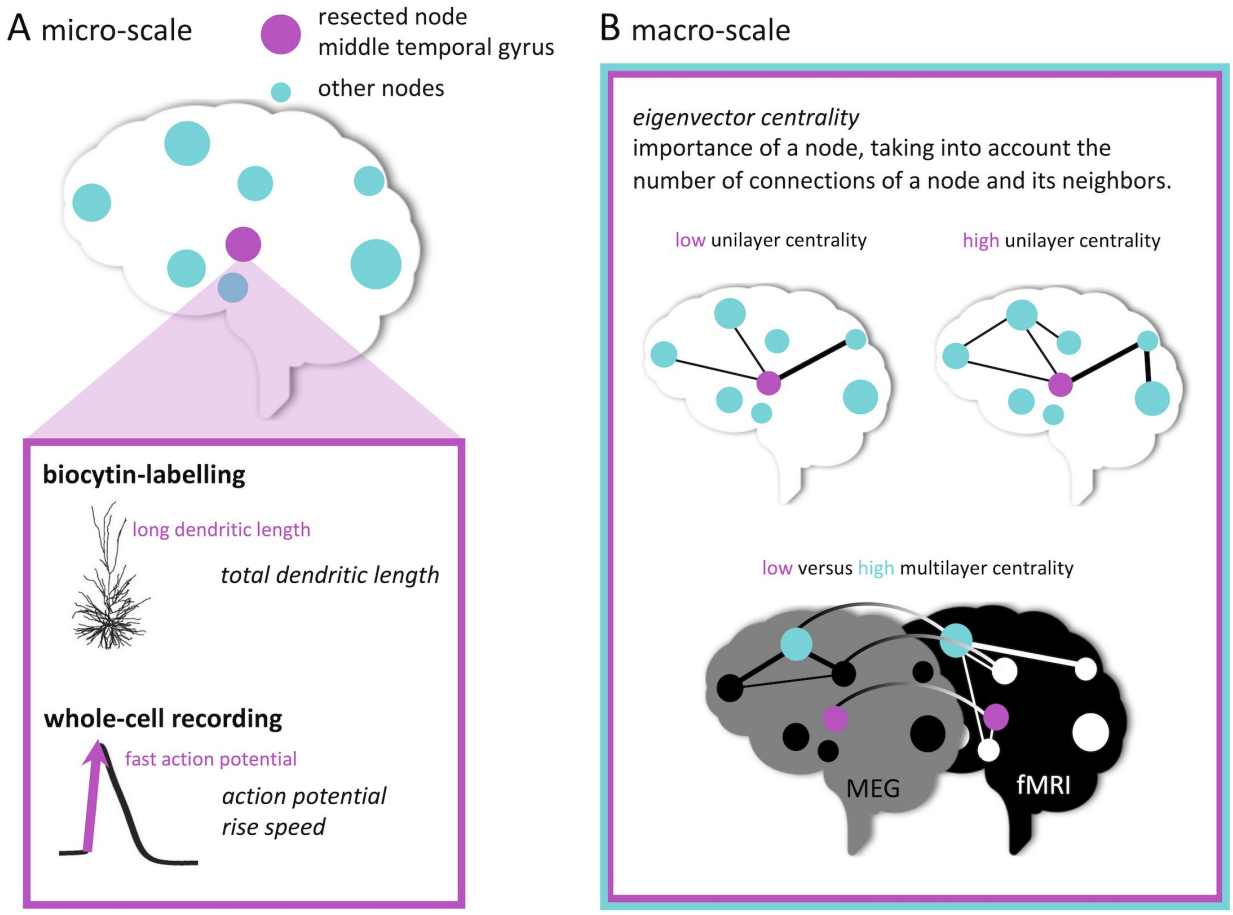

Legend. In (A), micro-scale tissue collection from the middle temporal gyrus (pink node) is depicted. Morphological analysis and electrophysiological recordings were performed. In (B), the macro-scale network measure of eigenvector centrality is illustrated for the unilayer (fMRI or MEG) and multilayer (combined fMRI and MEG) network analyses.

It has been considerably more difficult to assess micro-scale brain properties in relation to human cognitive variance. Memory disturbances in TLE have been related to micro-scale

properties of the (medial) temporal lobe in terms of protein expression [22]. Recently, morphological and physiological properties of individual neurons were shown to explain variance in intelligence in TLE patients [23]. Pyramidal neurons in resected non-pathological tissue from the non-pathological temporal cortex of patients with higher intelligence had larger, more complex dendrites and faster action potentials during high frequency activity. Larger dendrites may enable neurons to have more synaptic contacts, putatively playing more integrative roles than neurons with smaller dendrites [24,25]. Larger dendrites also directly influence the speed of action potential initiation, possibly providing these cells with better temporal resolution and more efficient information transfer [23,25,26]. Thus, regions that act as integrators for cognitive processes may be characterized by neurons with larger dendrites and faster action potentials.

Others have also started to hypothesize on possible links between micro-scale brain properties and macro-scale network profiles [27,28], with a recent review on "microstructure-informed connectomics" further underlining the potential for cross-linking between different scales in order to increase our understanding of the brain and treatment of disease [29]. These efforts are all the more relevant as large-scale initiatives like the Human Brain Project strive towards integration of our knowledge between these different scales of measurement. Indeed, studies have shown that regional variations in integration across scales go hand in hand: more integrative macro-scale brain regions as measured with diffusion weighted imaging tend to have bigger neurons with more axons than less integrative regions, as shown in animal and postmortem work [30,31]. Translation of these cross-scale associations to living humans, and their cognitive correlates, remain unknown.

Therefore, we investigated a unique cohort of TLE patients characterized at multiple scales. First, patients underwent cognitive assessments, neuroimaging and neurophysiological recording (fMRI and MEG [32,33]). Then, patients underwent neurosurgery and electrophysiological, patch-clamp recordings were performed on individual pyramidal neurons from the resected non-pathological temporal cortex tissue to characterize functional properties [23,34]. In parallel, dye labeling of recorded neurons enabled post-hoc quantification of neuronal morphology at (sub)cellular resolution. This pipeline allowed us to test whether individual differences covaried across scales, such that larger dendritic length and faster action potentials of the temporal region would associate with higher functional network centrality of this node. We also explored whether the macro-scale properties of the region related to individual differences in memory functioning, expecting greater centrality of this DMN region to relate to better memory performance.

Results

Patients

All patients undergoing resective neurosurgery for drug-resistant epilepsy localized at the medial temporal lobe between 2009-2016 at Amsterdam University Medical Centers (location VUmc, Amsterdam, The Netherlands) were eligible for participation. All patients underwent temporal lobectomy and were included in a previously published study [23]. In 15 of the 46 patients originally included, MEG and fMRI were not available. Finally, 31 patients (15 females) were included (see Table 1 on the next page for detailed characteristics per patient) with a mean age of 33 years (± 11 years).

A schematic of the analysis is provided in Figure 1 on page 6. The tissue collection as described in [23] formed the basis for further analyses (and see Materials and Methods for detailed information). In short, tissue exclusively originated from the middle temporal gyrus and was removed in order to gain access to the disease focus in deeper lying structures. In all patients, the resected neocortical tissue was not part of the epileptic focus or tumor and displayed no structural/functional abnormalities in presurgical MRI investigation or histological analysis by an experienced pathologist. This tissue was then analyzed with single cell electrophysiology and morphology, yielding a number of parameters. As our three measures of integration at the micro-scale, we selected total dendritic length, rise of the 1st action potential (AP), and APs fired at frequencies between 20-40 Hz (see Materials and Methods) for further cross-scale analysis, due to their proven relevance for intelligence in this patient cohort [23].

Table 1. Patient characteristics

ID	fMRI	MEG	Ephys	Morph	Sex	Age	Lat	Dom	Onset	Dur	Freq	Etiol	Type	AED	IR	DR	WMS
1	A	NA	A	A	F	21	R	Non	11	10	32	LGG	SP	LEV | VPA	49	10	85
2	A	NA	A	A	F	31	L	Non	16	15	13	LGG	CP	CBZ | LEV	55	6	100
3	A	A	A	A	F	29	L	Dom	13	17	32	HS	CP | GTC	LTG | TPM	48	5	NA
4	NA	A	A	A	M	20	R	Non	16	5	2	DNET	CP	CBZ | LEV	52	NA	NA
5	A	NA	A	A	F	27	R	Non	14	13	120	DNET	SP	CBZ | LTG	28	7	90
6	NA	A	A	NA	M	18	R	Non	1	17	150	HS	CP	OXC	NA	NA	NA
7	A	A	NA	A	F	23	L	NA	15	8	9	HS	SP | GTC	LEV | OXC	35	1	82
8	A	A	NA	A	M	53	L	Non	6	47	10	LGG	CP	CBZ | CLB	25	9	65
9	A	NA	NA	A	M	19	R	Non	17	2	450	GLI	CP	CLB | OXC	NA	NA	75
10	NA	A	NA	A	F	35	L	NA	1	34	1	NA	SP | CP | GTC	CZP | LCS | LTG | LEV	36	9	78
11	NA	A	NA	A	M	25	L	NA	9	16	2	HS	SP | CP | GTC	CLB | LCS | LEV	52	12	NA
12	NA	A	A	A	F	31	R	Dom	21	10	4	HS	CP	CBZ | CLB	41	1	80
13	NA	A	A	A	M	49	L	Dom	8	41	2	HS	CP	CBZ | CLB | LEV	45	9	NA
14	A	NA	A	A	F	45	R	Dom	23	22	3	HS	CP	CBZ | CLB | LTG	51	11	101
15	A	NA	A	NA	M	38	R	Non	28	10	6	HS	CP	CBZ	NA	NA	110
16	A	NA	A	NA	M	44	L	NA	35	9	4	HS	SP	LCS | VPA	NA	NA	102
17	NA	A	A	NA	M	53	L	Dom	18	35	4	NA	CP	CBZ	NA	NA	NA
18	NA	A	NA	A	F	30	L	NA	2	28	9	HS	CP | GTC	CLB | OXC	54	1	70
19	NA	A	A	A	M	44	L	NA	4	40	8	HS	CP | GTC	LTG | LEV	30	10	83
20	NA	A	A	NA	F	32	R	NA	6	26	151	MCD	NA	NA	NA	NA	NA
21	A	A	A	NA	F	41	R	Non	8	33	6	GLI	AB | CP	LEV | CBZ | VPA | CLB	44	NA	86
22	A	NA	A	NA	M	29	R	Non	23	7	5	NA	AB | CP	PHB | CBZ	28	NA	NA
23	A	A	A	NA	F	20	R	Non	4	17	6	MCD	CP	LEV | CBZ	58	NA	NA
24	NA	A	A	NA	M	21	L	NA	8	13	6	GG	AB	CBZ | LEV | LTG	NA	NA	84
25	NA	A	A	NA	F	48	R	NA	14	34	48	HS	AB | GTC	ZNS | CBZ | VPA	48	NA	104
26	A	NA	A	NA	M	44	R	Non	25	19	1	HS	CP	LTG | CBZ	NA	NA	NA
27	NA	A	A	NA	M	43	R	NA	6	37	7	HS	SP | CP	OXC | LEV	NA	NA	NA
28	A	A	A	NA	F	33	R	Non	19	14	150	HS	AB | CP	CBZ | LEV | CLB	51	NA	80
29	A	A	A	NA	M	51	R	Non	4	48	60	NA	CP | GTC	CBZ | PHB	41	NA	NA
30	A	A	A	A	F	18	R	Non	5	13	17	GG	CP	OXC	66	NA	NA
31	A	A	A	A	M	23	R	Non	11	12	8	HS	CP	OXC	56	NA	83

Legend. ID = identification number, fMRI = functional magnetic resonance imaging, MEG = magnetoencephalography, Ephys = electrophysiology, Morph = morphology, Lat = lateralization of epileptic focus, Dom = dominant hemisphere of resection, Onset = age in years at seizure onset, Dur = duration of epilepsy in years, Freq = frequency of seizures per month, Etiol = etiology of epilepsy, Type = type of epilepsy, AED = anti-epileptic drugs, IR = immediate recall on the Rey Auditory Verbal Learning Test, DR = delayed recall on the Rey Auditory Verbal Learning Test, WMS = Wechsler Memory Scale Verbal Memory Index, A = available, NA = not available, F = female, M = male, R = right, L = left, Non = non-dominant, Dom = dominant, LGG = low-grade glioma, HS = hippocampal sclerosis, DNET = dysembrionic neuroepithelial tumor, CAV = cavernoma, GLI = gliosis, MCD = malformation of cortical development, GG = ganglioglioma, SP = simpel partial, CP = complex partial, GTC = generalized tonic clonic, AB = absence, LEV = levetiracetam, VPA = valproic acid, CBZ = carbamazepine, CLB = clobazam, OXC = oxcarbazepine, LTG = lamotrigine, LCS = lacosamide, PHB = phenobarbital.

For fMRI and MEG analysis, the same structural MRI was used to coregister the functional data to, ensuring spatial comparability between modalities. For fMRI, we used standard and previously published pre-processing of pseudo resting-state data to extract extensively motion-corrected time series for all regions with reliable signal in an atlas spanning 78 regions of the cortex [35]. Pearson's correlations were used to construct the links between these nodes, yielding a single network per patient. For MEG, we used standard and previously published pre-processing of resting-state recordings and subsequent beamforming to extract time series from the same cortical regions [32,33]. Connections between these regions were constructing using the phase lag index [36], yielding a single network per patient. Centrality was then calculated for the region from which the tissue was taken specifically, for both the fMRI and MEG networks, as well as for a multilayer network that combined fMRI and MEG networks. Viewing different network modalities separately may decrease explanatory power of network measures [68–70]. Multilayer network theory [71,72] offers an analytical framework that allows for synergy between modalities to be captured. Each layer in a multilayer network represents a network characterized by one type of connectivity. Interlayer connections link the same region across different layers. Importantly, multilayer network measures supersede summed properties of individual layers when trying to explain system behavior [73,74]. Multilayer techniques have only recently been applied to neuroscience [37,38,75,76], but show promising results towards explaining more cognitive variance than unilayer analyses in Alzheimer's disease patients [10]. Ultimately, this yielded three centrality values per patient (fMRI, MEG, multilayer).

Finally, patients underwent cognitive assessments during presurgical workup, as reported on before [23]. As our three measures of verbal memory, we selected (1) the composite Verbal

Memory Index of the Wechsler Memory Scale (WMS [66]), and (2) immediate and (3) delayed recall of the Dutch version of Rey's Auditory Verbal Learning Test (RAVLT [67]). Higher values indicate better memory performance (see Materials and Methods for detailed information).

Sample sizes varied per scale, as indicated in Table 1. We therefore first performed multiple imputation of missing data based on patterns of covariation within the available data [82], namely (1) the three micro-scale measures per patient (TDL, AP rise speed (1st), and AP rise speed (20-40Hz)), (2) the three macro-scale centrality values per patient (MEG, fMRI and multilayer), and (3) the three memory scores per patient (WMS, RAVLT immediate and delayed recall). We thereby created ten imputed datasets, on which we performed cross-scale canonical correlation analyses to test our primary hypotheses. If significant, these canonical correlation analyses were then followed by correlational analysis on the non-imputed samples.

Associations between micro-scale and macro-scale brain properties

We first asked whether longer TDLs and faster APs, hypothetically signs of greater integrative potential at the micro-scale, generally related to greater macro-scale network centrality of the resected region, as such a correlation would indicate that integrative properties are preserved across scales. Indeed, there was a significant cross-scale correlation in the imputed data (canonical correlation coefficient = 0.329, $F(9,740) = 7.339$, $p < 0.001$, $n = 31$).

We then investigated pairwise correlations in non-imputed data (Figure 2 on page 14). Longer micro-scale TDL was significantly related to greater macro-scale fMRI centrality (rho = 0.758, CI [0.115 0.975], $p = 0.016$, $n = 10$; Figure 3A on page 16). This association remained significant when creating a sample-specific distribution of the correlation through permutation

analysis (rho cut-off = 0.636, Figure 3B left). We then performed leave-one-out analyses, where we iteratively excluded a single patient from the correlation analysis to see whether this result was driven by individual data point. This yielded significant results in 7 of 10 analyses (Figure 3B middle). Finally, we explored whether micro-scale TDL of the resected region also correlated with macro-scale centrality of other cortical regions. This analysis revealed a significant negative correlation between micro-scale TDL of the resected region and macro-scale fMRI centrality of the ipsilateral paracentral lobule (rho = -0.721, p = 0.024, Figure 3B right), although this result did not survive correction for the 36 correlations tested.

Furthermore, faster micro-scale AP rise speed (1st) was significantly related to greater macro-scale fMRI centrality (rho = 0.539, CI [0.042 0.868], p = 0.041, n = 15; Figure 3C/D). This finding remained in permutation testing (rho cut-off = 0.525), but was mostly non-significant in leave-one-out analyses. Spatially, micro-scale AP rise speed (1st) of the resected area was also significantly associated with macro-scale fMRI centrality of the precentral region (rho = 0.582, p = 0.025). Moreover, there were significant negative relationships with fMRI centrality of the superior parietal region (rho = -0.657, p = 0.010) and temporal pole (rho = -0.611, p = 0.018), although these correlations did not survive correction for multiple comparisons.

The only pairwise correlation that survived correction for the nine pairwise tests performed between micro-scale and macro-scale characteristics of the resected region was the significant positive association between micro-scale AP rise speed (1st) and macro-scale multilayer centrality (rho = 0.964, CI [0.698 1.000], p < 0.001, n = 7; Figure 4A on page 18). Moreover, this association was robust in permutation and leave-one-out analyses, and was spatially specific, also when not correcting for multiple comparisons.

Figure 2. All pairwise correlations

	fMRI centrality	MEG centrality	multilayer centrality
total dendritic length	**0.758 (0.016) | 10**	0.441 (0.154) | 12	0.300 (0.683) | 5
AP rise speed (1st)	**0.539 (0.041) | 15**	0.025 (0.928) | 17	**0.964 (0.0028) | 7**
AP rise speed (20-40Hz)	0.229 (0.411) | 15	0.407 (0.106) | 17	0.107 (0.840) | 7
complete subgroup total dendritic length	0.700 (0.233) | 5	0.400 (0.517) | 5	0.300 (0.683) | 5
complete subgroup AP rise speed (1st)	0.571 (0.200) | 7	0.357 (0.444) | 7	**0.964 (0.0028) | 7**
complete subgroup AP rise speed (20-40Hz)	0.536 (0.236) | 7	0.464 (0.302) | 7	0.107 (0.840) | 7
WMS verbal	-0.126 (0.697) | 12	0.169 (0.620) | 11	0.500 (0.450) | 5
RAVLT immediate	-0.430 (0.125) | 14	0.473 (0.055) | 17	0.017 (0.982) | 9
RAVLT delayed	**0.857 (0.024) | 7**	0.224 (0.567) | 9	0.500 (1.000) | 3

legend

rho (p-value) | n	small negative association
rho (p-value) | n	medium negative association
rho (p-value) | n	small positive association
rho (p-value) | n	medium positive association
rho (p-value) | n	large positive association
rho (p-value) | n	significant positive association
rho (p-value) | n	significant positive association after Bonferroni correction

Legend. This figure shows an overview of all associations between micro-scale properties and macro-scale properties (top three rows), as well as between macro-scale properties and memory functioning (bottom three rows), using the maximum samples of patients with available data. Additionally, the middle three rows (in gray) reflect all pairwise correlations between micro-scale and macro-scale properties when considered in the same subgroup with complete macro-scale data for the morphological (n = 5) and

electrophysiological (n = 7) analyses. Green elements reflect positive correlations (with rho, p and n in text), ranging from small correlations (rho < 0.4, light green) to medium correlations (0.4 < rho < 0.6, medium green) to large correlations (rho > 0.6, dark green). White, bold text indicates statistical significance (P < 0.05) and very dark green elements with white, bold text indicates statistical significance after Bonferroni correction for multiple (nine) comparisons. Blue elements reflect negative correlations in the same way. fMRI = functional Magnetic Resonance Imaging, MEG = magnetoencephalography, AP = action potential, WMS = Wechsler Memory Scale, RAVLT immediate = Rey Auditory Verbal Learning Test immediate recall, RAVLT immediate = Rey Auditory Verbal Learning Test delayed recall. In (B), we only select patients with both macro-scale modalities and either of the micro-scale measures available, namely five patients with total dendritic length and seven patients with action potential rise speed. The legend is identical between (A) and (B).

Figure 3. Significant pairwise associations between micro-scale and macro-scale properties

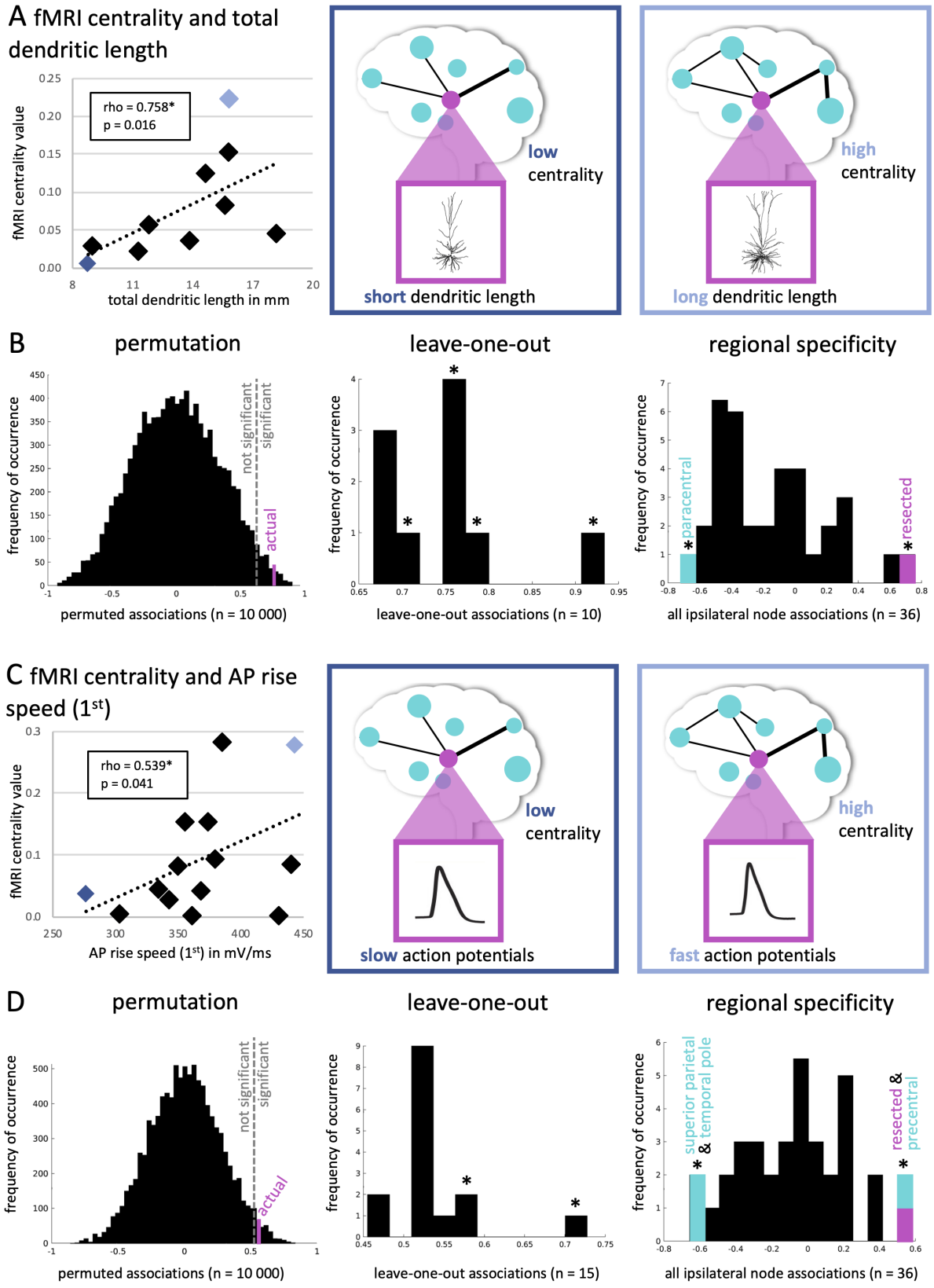

Legend. (A) Displays a scatter plot of the significantly positive correlation between total dendritic length (in mm) and functional Magnetic Resonance Imaging (fMRI) centrality. The dark blue diamond in the plot represents a single patient, who has low centrality and short dendritic length (schematically depicted in the middle panel), while the light blue diamond represents a patient with high centrality and long dendritic length (right panel). In (B), the analyses of the robustness of these results are displayed. The left panel shows the distribution of permuted correlations (10 000 permutations), with the actual (pink) association being smaller than the alpha = 0.05 threshold indicated by the dotted line. The middle panel displays the 10 leave-one-out associations in addition to the real correlation, yielding a significant correlation in 7 of 10 analyses as indicated by the asterisks. The right panel displays all correlations between ipsilateral macro-scale centrality values (n = 36 regions) and total dendritic length of the resected area. The reported positive association (with the resected region) in pink as well as the negative correlation between paracentral centrality and total dendritic length are significant. In (C), a scatter plot of the significantly positive correlation between action potential (AP) rise speed (1st) and fMRI centrality is shown. In (D), the analyses of the robustness of these results are displayed in the same manner as in (B).

Figure 4. Significant pairwise association between micro-scale and macro-scale properties after correction for multiple comparisons

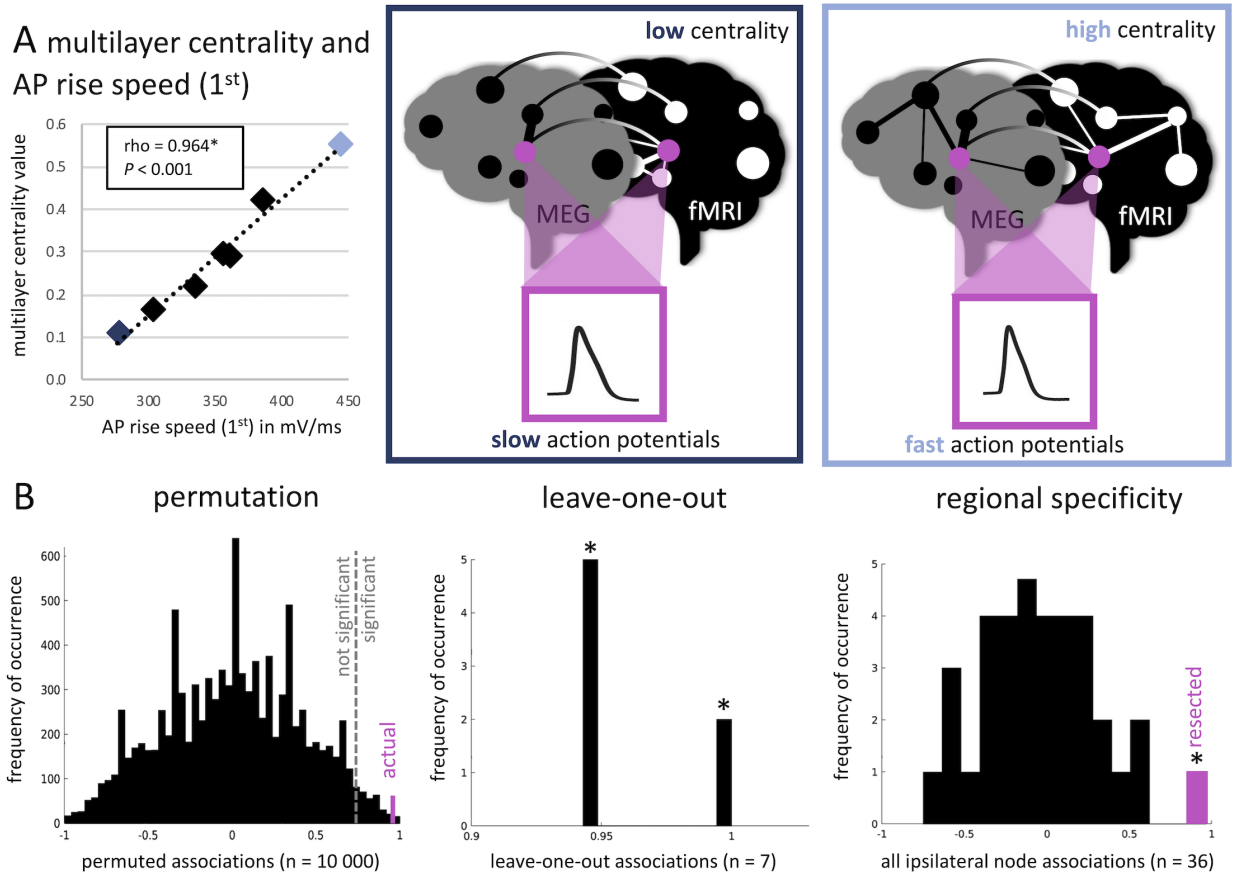

Legend. (A) Displays a scatter plot of the significantly positive correlation between action potential (AP) rise speed (1st) and multilayer centrality, which is the only pairwise association significant after Bonferroni correction for multiple comparisons. The dark blue diamond in the plot represents a single patient, who has low centrality and slow action potentials (schematically depicted in the middle panel), while the light blue diamond represents a patient with high centrality and fast action potentials (right panel). In (B), the analyses of the robustness of these results are displayed. The left panel shows the distribution of permuted correlations (10 000 permutations), with the actual (pink) association being smaller than the alpha = 0.05 threshold indicated by the dotted line. The middle panel displays the 7 leave-one-out associations in addition to the real correlation, yielding a significant correlation in all analyses as indicated by the asterisks.

The right panel displays all correlations between ipsilateral macro-scale centrality values (n = 36 regions) and AP rise speed (1st) of the resected area. The reported positive association (with the resected region) in pink is the only significant correlation.

Since different numbers of patients were available for each pairwise correlation depending on modalities available, we also investigated whether the small subset of patients with complete data showed the same patterns of correlation as the larger but heterogeneous samples. Indeed, Figure 2 also shows the associations of both unilayer and multilayer network indices with micro-scale measures in the same samples of 5 patients (for TDL) and 7 patients (for AP rise speeds). As was the case for the mixed samples, only multilayer centrality and AP rise speed (1st) were significantly correlated in this complete dataset, indicating that patient selection differences between the above described subsamples did not confound the reported pairwise correlations.

From network centrality to memory functioning

Finally, we investigated the links between macro-scale network topology of the resected region and memory functioning. A significant canonical correlation was found between centralities of the resected region and memory functioning (canonical correlation coefficient = 0.234, $F(12,670) = 2.14$, $p = 0.013$), such that greater centrality related to better memory functioning.

Unfortunately, very few patients had complete data across these scales, rendering the pairwise testing of associations greatly underpowered. Only greater fMRI centrality was significantly related to greater RAVLT delayed recall (rho = 0.857, CI [0.373 1.000], $p = 0.024$, $n = 7$; Figure 2).

Discussion

We report on a unique cohort of TLE patients with data spanning multiple scales of investigation. Confirming our hypotheses, individual differences in cellular properties of neurons stemming from the non-pathological lateral temporal lobe correlated with differences in macro-scale functional network centrality of the larger brain region that these neurons were taken from. Patients with longer dendrites and faster action potentials, indication of more integrative potential at the micro-scale, also displayed more integrative profiles of this region in the macro-scale brain network. Finally, variations in network centrality of the resected brain region seemed associated with individual differences in memory functioning.

Previous work has reported that more integratively connected (as measured with diffusion imaging) macro-scale brain regions tend to have bigger neurons with more axons, while locally connected brain regions are made up of smaller neurons that are connected with lower axonal density [30,31]. Interestingly, these studies were performed in postmortem human donors with multiple sclerosis [30] or macaques [31], suggesting that such cross-scale correlations between morphology and network profile may not be specific to TLE, but an evolutionary conserved organizational principle across species. The strength of the current study is that we combined functional and structural micro-scale parameters (action potential kinetics and full morphologies) with functional macro-scale network analysis in the same subjects, an approach not possible in postmortem donors. We found that individuals with more complex neuronal morphology of the lateral temporal lobe (i.e. longer total dendritic length) and faster action potentials also have greater network centrality at that location. Specifically, this association was present between the micro-scale measures and fMRI centrality, while only the relationship between AP rise speed (1st)

and multilayer centrality survived correction for multiple comparisons. This finding suggests that multilayer centrality may capture micro-scale electrophysiological properties of the tissue better than either of the two modalities (fMRI and MEG) alone, which may be in line with other multilayer brain network studies [37,38]. It should, however, be noted that the lack of significance for unilayer network profiles as well as the significance of the multilayer network profile may reflect limited statistical power in these small samples.

We further hypothesized that individual differences in network profiles of the resected DMN region would correlate with memory functioning, which was confirmed by canonical correlation analysis on imputed datasets, corroborating previous work in TLE patients [18–21]. With limited statistical power in pairwise associations, we report only a significant correlation between fMRI centrality and RAVLT delayed recall. Future studies are necessary to assess the specificity of these findings for modalities and memory subtests.

Several limitations of this study should be noted. First and foremost, the uniqueness of this multi-scale dataset meant that only a small sample was available, also precluding subgroup analysis or exploration of confounders that might have affected the current results, e.g. lateralization of the epileptogenic zone, sex, and age. It is also impossible to use a control group for this analysis: healthy individuals can obviously not be subjected to the micro-scale measurements we report on. Another limitation is the spatial resolution of matching between the micro-scale and macro-scale analyses: while certainty about the location of origin of the resected tissue was in the order of millimeters, the atlas region used to reflect the tissue location spans several centimeters. We chose this atlas as it has been used successfully by our group in previous

studies with comparable patient populations and thus has proven cognitive and cellular relevance [35,39–44], but future studies may aim to match tissue locations with increased spatial accuracy.

In conclusion, we show that individual differences in micro-scale cell anatomy and functioning relate to macro-scale network centrality of the temporal lobe in epilepsy patients, the latter of which correlates with memory functioning. These results underline the translational nature of individual differences between epilepsy patients, going from cell via network topology to cognition. Ultimately, better understanding of these cross-scale individual differences may lead the way to better treatment of neurological disease in general [29], and of memory deficits in TLE patients specifically.

Materials and Methods

Patients

All procedures were performed with the approval of the Medical Ethical Committee of VUmc, and in accordance with Dutch license procedures and the Declaration of Helsinki. Written informed consent was provided by all subjects for data and tissue use for scientific research. Patients did not consent to sharing their raw data. However, the full derived variable set used for statistical analysis in the current work is available from GitHub (https://github.com/multinetlab-amsterdam/projects/tree/master/multiscale_integration), where our code can also found.

Single cell electrophysiology and morphology

Upon surgical resection, the cortical tissue was immediately transferred to ice-cold artificial cerebral spinal fluid, then transported to the electrophysiology lab within 15 mins, where neocortical slices (350µm thickness) were prepared (see [23] for details). Whole-cell patch-clamp recordings were made of layer 2 and layer 3 pyramidal neurons and action potentials (APs) were elicited by incrementing step current injections (step size 30–50 pA). Waveforms were sorted according to their instantaneous firing frequency (1/time to previous AP) and AP rise speed was defined as the peak of AP derivative (dV/dt) for all APs from all neurons from each subject. The rise speed of the 1st AP and APs fired at frequencies between 20-40 Hz were used, as these have previously been associated with intelligence [23].

During electrophysiological recordings, cells were loaded with biocytin through the recording pipette. After recording, slices were fixed in 4% paraformaldehyde and cells were revealed with chromogen 3,3-diaminobenzidine (DAB) tetrahydrochloride using the avidin–

biotin–peroxidase method [45]. Neurons were digitally reconstructed using Neurolucida software (Microbrightfield, Williston, VT, USA). Only neurons with virtually complete dendritic structures were included [34,46]. For each neuron, we extracted total dendritic length (TDL) of all basal and apical dendrites and then averaged these data (1 to 10 neurons per patient).

Macro-scale structural imaging

MRI was performed on a 1.5T magnet (Siemens Sonata) and included an anatomical 3D T1-weighted MPRAGE scan (sequence parameters: TR = 2700ms, TE = 5.2ms, TI = 950ms, 1mm isotropic resolution, 176 slices). Imaging processing was performed using FSL5 (http://www.fmrib.ox.ac.uk/fsl). Standard FSL procedures were used to preprocess structural imaging: non-brain tissue was removed from the 3D T1-weighted images using the Brain Extraction Tool [47], and grey and white matter segmentation was performed using FAST [48]. Non-brain tissue was removed and tissue segmentation was performed. To construct each individual's functional brain network, the Automated Anatomical Labeling atlas was used to define 78 cortical regions [49]. This atlas was warped from standard space to native space, and masked with each subject's native grey matter mask.

Functional magnetic resonance imaging

Patients underwent presurgical fMRI for language localization. Previous studies have shown that the intraindividual effect of any task or state on network topology is small in comparison to interindividual differences in network topology [50], indicating that we may use these pseudo resting-state data to extract individual network signatures that largely generalize outside the

specific task performed in this cohort. Others and we ourselves have previously used resting-state analysis on such task data for network analysis in both healthy controls and patients [35,51,52].

Scanning was performed using a standard echo-planar imaging sequence (TR = 2850ms, TE = 60ms, 144 volumes, 3.3mm isotropic resolution, 7min). During the scan, patients performed a language task in which nine volumes of word generation were alternated with nine volumes of rest (imagery of a landscape).

Preprocessing was performed using standard procedures [53], including discarding the first five volumes, motion correction, spatial smoothing, and high-pass filtering. Six regions with low signal quality (mainly orbitofrontal areas) were excluded, leaving 72 cortical regions for analysis. Additionally, ICA-AROMA was applied to minimize the impact of movement [54]. Functional images were co-registered to the anatomical scans [55]. Time series were extracted from the centroids of all regions, after which a 72x72 connectivity matrix per subject was created using Pearson correlation coefficients. Finally, the absolute values of these correlations were used as weighted connectivity. Further details can be found in the Supplementary Information.

Magnetoencephalography

Patients underwent resting-state MEG as part of their presurgical work-up and/or in the setting of scientific research ([32,33]). Interictal eyes-closed recordings were acquired in supine position using a whole-head system (Elekta Neuromag Oy, Helsinki, Finland) with 306 channels inside a magnetically shielded room (Vacuumschmelze GmbH, Hanau, Germany). Data were recorded with a sampling frequency of 1250Hz, filtered online with a 410Hz anti-aliasing filter and a 0.1Hz high-pass filter. The head position relative to the sensors was recorded continuously with head-

localization coils. A 3D digitizer (Fastrak, Polhemus, Colchester, VT, USA) digitized the head-localization coil positions and scalp outline (roughly 500 points) to allow surface matching of the scalp surface points with anatomical MRI.

Three eyes-closed resting-state recordings of typically 15 min each were recorded for clinical analysis of interictal epileptiform activity. Only one recording was analyzed in this study and chosen according to the following criteria with descending priority: (1) consisting of at least 5 minutes of data, (2) displaying the smallest number of artifacts as per visual inspection, and (3) being the earlier dataset of the three recordings.

Further analysis of these data has been extensively described before [33]. Offline spatial filtering of the raw data removed artifacts using the temporal extension of Signal Space Separation (tSSS [56]) using MaxFilter software (Elekta Neuromag Oy; version 2.1), with details and parameter settings as described in [57]. The reconstruction of neuronal sources was performed with an atlas-based beamforming approach, modified from [58]. The time series (virtual electrodes) for each centroid of each atlas region were reconstructed [59]. These time series were then filtered in the theta band (4-8Hz), because of its proven relevance for cognitive functioning in these patients [60,61] and to limit the number of investigated variables in this limited sample.

As a measure of functional connectivity, the phase lag index (PLI) was used [36]. The PLI assesses the phase-relationship between two regions by quantifying the asymmetry in the distribution of instantaneous phase differences between two time series. It is robust against zero-lag phase synchronization due to volume conduction or field spread [62]. This analysis yielded a 78x78 MEG connectivity matrix per patient.

Network analysis

We then created minimum spanning trees (MSTs) to extract the functional backbone of each fMRI and MEG network and allow for comparison between patients and modalities [32,63–65]. The MST is a binary network that connects all nodes in a network without forming cycles while maximizing connectivity strength. Eigenvector centrality was then calculated per brain region. Of note, there is a plethora of network measures that measure integration and segregation, which are highly intercorrelated (see for instance [66]). Instead of using multiple measures in this small sample with limited statistical power, we chose to focus on eigenvector centrality. Eigenvector centrality is a spectral centrality measure, that not only takes into account the number of connections of a node, but also weighs the number of connections of its neighboring nodes [67].

We then used the fMRI and MEG MSTs to construct a two-layer network consisting of the 72 nodes available in both modalities [77], where each region was connected only to itself across the two layers, forming an interconnected binary multiplex. We then calculated multilayer eigenvector centrality per region [78].

All analyses were performed using in-house scripts in Python, in combination with the Brain Connectivity Toolbox [79] implemented in Matlab R2012a (Mathworks, Natick, MA, USA).

Memory functioning

Patients underwent cognitive assessments during presurgical workup as has been reported before [23]. In order to assess verbal memory functioning, in particular because of its relevance both in terms of tissue location in the DMN and incidence of cognitive deficits, the Wechsler

Memory Scale (WMS [80]) and the Dutch version of Rey's Auditory Verbal Learning Test (RAVLT [81]) were selected for analysis in the current work. From the WMS, the composite Verbal Memory Index was used, which has a mean value of 100 with a standard deviation of 15 in a normative, healthy population. From the RAVLT, immediate recall in terms of total correctly encoded words across five trials (15 words each) was quantified, with possible scores ranging between 0-75 words in total. Additionally, delayed recall of the 15 words was assessed after 15mins, yielding an additional outcome measure of memory retrieval. Higher values indicate better memory performance.

Statistical analysis

Statistical analysis was performed using SPSS Statistics (IBM Corporation, Armonk, NY, USA). Cross-scale pairwise associations in non-imputed data were tested using non-parametric Spearman's correlation coefficients with bootstrapping (1 000 samples, 95% confidence intervals (CI)). When significant, robustness was explored by permuting the micro-macro pairs to create a data-specific correlation distribution (10 000 permutations) and by leave-one-out analysis. Spatial specificity of the associations was explored by correlating the micro-scale measure with macro-scale centralities of all other ipsilateral nodes in the network. Pairwise associations between macro-scale centralities and memory were tested using Spearman's correlation coefficients. The threshold for statistical significance was set at two-tailed alpha < 0.05, but we also report significant results after applying Bonferroni correction for multiple comparisons.

References

1. Aronica E, Mühlebner A. Neuropathology of epilepsy. Handbook of Clinical Neurology. Elsevier B.V.; 2018. pp. 193–216. doi:10.1016/B978-0-12-802395-2.00015-8
2. Ahmed R, Rutka JT. The role of MEG in pre-surgical evaluation of epilepsy: current use and future directions. Expert Review of Neurotherapeutics. Taylor and Francis Ltd; 2016. pp. 795–801. doi:10.1080/14737175.2016.1181544
3. Witt JA, Helmstaedter C. Cognition in epilepsy: Current clinical issues of interest. Current Opinion in Neurology. Lippincott Williams and Wilkins; 2017. pp. 174–179. doi:10.1097/WCO.0000000000000430
4. Stam CJ. Modern network science of neurological disorders. Nat Rev Neurosci. 2014;15: 683–95. doi:10.1038/nrn3801
5. Bassett DS, Sporns O. Network neuroscience. Nat Neurosci. 2017;20: 353–364. doi:10.1038/nn.4502
6. van den Heuvel MP, Stam CJ, Kahn RS, Hulshoff Pol HE. Efficiency of functional brain networks and intellectual performance. J Neurosci. 2009;29: 7619–7624.
7. van Mierlo P, Höller Y, Focke NK, Vulliemoz S. Network Perspectives on Epilepsy Using EEG/MEG Source Connectivity. Front Neurol. Frontiers Media SA; 2019;10. doi:10.3389/fneur.2019.00721
8. Caciagli L, Bernhardt BC, Hong SJ, Bernasconi A, Bernasconi N. Functional network alterations and their structural substrate in drug-resistant epilepsy. Frontiers in Neuroscience. Frontiers Media S.A.; 2014. doi:10.3389/fnins.2014.00411
9. De Domenico M, Sole-Ribalta A, Cozzo E, Kivela M, Morena Y, Porter MA, et al.

Mathematical formulation of multilayer networks. Phys Rev X. 2013;3: 041022.

10. Yu M, Engels MMA, Hillebrand A, Van Straaten ECW, Gouw AA, Teunissen C, et al. Selective impairment of hippocampus and posterior hub areas in Alzheimer's disease: An MEG-based multiplex network study. Brain. Oxford University Press; 2017;140: 1466–1485. doi:10.1093/brain/awx050

11. Horien C, Greene AS, Constable RT, Scheinost D. Regions and Connections: Complementary Approaches to Characterize Brain Organization and Function. Neurosci. SAGE PublicationsSage CA: Los Angeles, CA; 2019; 107385841986011. doi:10.1177/1073858419860115

12. Deco G, Tononi G, Boly M, Kringelbach ML. Rethinking segregation and integration: Contributions of whole-brain modelling. Nature Reviews Neuroscience. Nature Publishing Group; 2015. pp. 430–439. doi:10.1038/nrn3963

13. Cohen JR, D'Esposito M. The segregation and integration of distinct brain networks and their relationship to cognition. J Neurosci. Society for Neuroscience; 2016;36: 12083–12094. doi:10.1523/JNEUROSCI.2965-15.2016

14. Bertolero MA, Yeo BTT, D'Esposito M. The diverse club. Nat Commun. 2017;8: 1277.

15. van den Heuvel MP, Sporns O. Rich-club organization of the human connectome. J Neurosci. 2011;31: 16775–15786.

16. Meador KJ. Cognitive outcomes and predictive factors in epilepsy. Neurology. 2002;58: S21-6.

17. Raichle ME, MacLeod AM, Snyder AZ, Powers WJ, Gusnard DA, Shulman GL. A default mode of brain function. Proc Natl Acad Sci U S A. 2001;98: 676–682.

18. DeSalvo M, Douw L, Tanaka N, Reinsberger C, Stufflebeam SM. Altered structural connectome in temporal lobe epilepsy. Radiology. 2014;270: 842–848.

19. Douw L, Leveroni CL, Tanaka N, Emerton BC, Cole AC, Reinsberger C, et al. Loss of Resting-State Posterior Cingulate Flexibility Is Associated with Memory Disturbance in Left Temporal Lobe Epilepsy. PLoS One. Public Library of Science; 2015;10: e0131209. doi:10.1371/journal.pone.0131209

20. McCormick C, Protzner AB, Barnett AJ, Cohn M, Valiante TA, McAndrews MP. Linking DMN connectivity to episodic memory capacity: What can we learn from patients with medial temporal lobe damage? NeuroImage Clin. 2014;5: 188–96. doi:10.1016/j.nicl.2014.05.008

21. Voets NL, Zamboni G, Stokes MG, Carpenter K, Stacey R, Adcock JE. Aberrant functional connectivity in dissociable hippocampal networks is associated with deficits in memory. J Neurosci. 2014;34: 4920–8. doi:10.1523/JNEUROSCI.4281-13.2014

22. Karádi K, Janszky J, Gyimesi C, Horváth Z, Lucza T, Dóczi T, et al. Correlation between calbindin expression in granule cells of the resected hippocampal dentate gyrus and verbal memory in temporal lobe epilepsy. Epilepsy Behav. 2012;25: 110–119. doi:10.1016/j.yebeh.2012.06.007

23. Goriounova NA, Heyer DB, Wilbers R, Verhoog MB, Giugliano M, Verbist C, et al. Large and fast human pyramidal neurons associate with intelligence. Elife. 2018;7. doi:10.7554/eLife.41714

24. Poirazi P, Brannon T, Mel BW. Pyramidal neuron as two-layer neural network. Neuron. 2003;37: 989–99. doi:10.1016/s0896-6273(03)00149-1

25. Eyal G, Mansvelder HD, de Kock CPJ, Segev I. Dendrites Impact the Encoding Capabilities of the Axon. J Neurosci. 2014;34: 8063–8071. doi:10.1523/JNEUROSCI.5431-13.2014

26. Testa-Silva G, Verhoog MB, Linaro D, de Kock CPJ, Baayen JC, Meredith RM, et al. High bandwidth synaptic communication and frequency tracking in human neocortex. PLoS Biol. 2014;12: e1002007. doi:10.1371/journal.pbio.1002007

27. Sporns O. Connectome networks: From cells to systems. Research and Perspectives in Neurosciences. Springer Verlag; 2016. pp. 107–127. doi:10.1007/978-3-319-27777-6_8

28. van den Heuvel MP, Yeo BTT. A Spotlight on Bridging Microscale and Macroscale Human Brain Architecture. Neuron. Elsevier; 2017;93: 1248–1251. doi:10.1016/j.neuron.2017.02.048

29. Larivière S, Vos De Wael R, Paquola C, Hong SJ, Mišić B, Bernasconi N, et al. Microstructure-informed connectomics: Enriching large-scale descriptions of healthy and diseased brains. Brain Connect. Mary Ann Liebert Inc.; 2019;9: 113–127. doi:10.1089/brain.2018.0587

30. Kiljan S, Meijer KA, Steenwijk MD, Pouwels PJW, Schoonheim MM, Schenk GJ, et al. Structural network topology relates to tissue properties in multiple sclerosis. J Neurol. 2019;266: 212–222. doi:10.1007/s00415-018-9130-2

31. Scholtens LH, Schmidt R, de Reus MA, van den Heuvel MP. Linking macroscale graph analytical organization to microscale neuroarchitectonics in the macaque connectome. J Neurosci. 2014;34: 12192–205. doi:10.1523/JNEUROSCI.0752-14.2014

32. Nissen IA, Stam CJ, van Straaten ECW, Wottschel V, Reijneveld JC, Baayen JC, et al. Localization of the Epileptogenic Zone Using Interictal MEG and Machine Learning in a

Large Cohort of Drug-Resistant Epilepsy Patients. Front Neurol. 2018;9: 647. doi:10.3389/fneur.2018.00647

33. Nissen IA, Stam CJ, Reijneveld JC, van Straaten IECW, Hendriks EJ, Baayen JC, et al. Identifying the epileptogenic zone in interictal resting-state MEG source-space networks. Epilepsia. 2017;58: 137–148. doi:10.1111/epi.13622

34. Mohan H, Verhoog MB, Doreswamy KK, Eyal G, Aardse R, Lodder BN, et al. Dendritic and Axonal Architecture of Individual Pyramidal Neurons across Layers of Adult Human Neocortex. Cereb Cortex. 2015;25: 4839–53. doi:10.1093/cercor/bhv188

35. Derks J, Dirkson AR, de Witt Hamer PC, van Geest Q, Hulst HE, Barkhof F, et al. Connectomic profile and clinical phenotype in newly diagnosed glioma patients. NeuroImage Clin. 2017;14. doi:10.1016/j.nicl.2017.01.007

36. Stam CJ, Nolte G, Daffertshofer A. Phase lag index: Assessment of functional connectivity from multi channel EEG and MEG with diminished bias from common sources. Hum Brain Mapp. 2007;28: 1178–1193.

37. Battiston F, Nicosia V, Chavez M, Latora V. Multilayer motif analysis of brain networks. Chaos An Interdiscip J Nonlinear Sci. 2017;27: 047404. doi:10.1063/1.4979282

38. De Domenico M. Multilayer modeling and analysis of human brain networks. Gigascience. 2017;6: 1–8. doi:10.1093/gigascience/gix004

39. van Dellen E, de Witt Hamer PC, Douw L, Klein M, Heimans JJ, Stam CJ, et al. Connectivity in MEG resting-state networks increases after resective surgery for low-grade glioma and correlates with improved cognitive performance. NeuroImage Clin. 2012;2: 1–7. doi:10.1016/j.nicl.2012.10.007

40. Douw L, Groot M de, van Dellen E, Aronica E, Heimans JJ, Klein M, et al. Local MEG networks: the missing link between protein expression and epilepsy in glioma patients? Neuroimage. 2013;75: 195–203. doi:10.1016/j.neuroimage.2013.02.067

41. Carbo EWS, Hillebrand A, Van Dellen E, Tewarie P, De Witt Hamer PC, Baayen JC, et al. Dynamic hub load predicts cognitive decline after resective neurosurgery. Sci Rep. 2017;7. doi:10.1038/srep42117

42. van Dellen E, Douw L, Hillebrand A, de Witt Hamer PC, Baayen JC, Heimans JJ, et al. Epilepsy surgery outcome and functional network alterations in longitudinal MEG: a minimum spanning tree analysis. Neuroimage. 2014;86: 354–63. doi:10.1016/j.neuroimage.2013.10.010

43. Derks J, Kulik S, Wesseling P, Numan T, Hillebrand A, de Witt Hamer P, et al. Understanding cognitive functioning in diffuse glioma patients: the relevance of IDH mutation status and functional connectivity. Brain Behav. 2019;In press.

44. Derks J, Wesseling P, Carbo E, Hillebrand A, van Dellen E, de Witt Hamer PC, et al. Oscillatory brain activity associates with neuroligin-3 expression and predicts progression free survival in patients with diffuse glioma. J Neurooncol. 2018;https://do.

45. Horikawa K, Armstrong WE. A versatile means of intracellular labeling: injection of biocytin and its detection with avidin conjugates. J Neurosci Methods. Elsevier; 1988;25: 1–11. doi:10.1016/0165-0270(88)90114-8

46. Deitcher Y, Eyal G, Kanari L, Verhoog MB, Atenekeng Kahou GA, Mansvelder HD, et al. Comprehensive Morpho-Electrotonic Analysis Shows 2 Distinct Classes of L2 and L3 Pyramidal Neurons in Human Temporal Cortex. Cereb Cortex. 2017;27: 5398–5414.

doi:10.1093/cercor/bhx226

47. Smith SM. Fast robust automated brain extraction. Hum Brain Mapp. 2002;17: 143–55. doi:10.1002/hbm.10062

48. Zhang Y, Brady M, Smith S. Segmentation of brain MR images through a hidden Markov random field model and the expectation-maximization algorithm. IEEE Trans Med Imaging. 2001;20: 45–57. doi:10.1109/42.906424

49. Tzourio-Mazoyer N, Landeau B, Papathanassiou D, Crivello F, Etard O, Delcroix N, et al. Automated anatomical labeling of activations in SPM using a macroscopic anatomical parcellation of the MNI MRI single-subject brain. Neuroimage. 2002;15: 273–89. doi:10.1006/nimg.2001.0978

50. Gratton C, Laumann TO, Nielsen AN, Greene DJ, Gordon EM, Gilmore AW, et al. Functional Brain Networks Are Dominated by Stable Group and Individual Factors, Not Cognitive or Daily Variation. Neuron. 2018;98: 439-452.e5. doi:10.1016/j.neuron.2018.03.035

51. Krienen FM, Yeo BTT, Buckner RL. Reconfigurable task-dependent functional coupling modes cluster around a core functional architecture. Philos Trans R Soc Lond B Biol Sci. 2014;369. doi:10.1098/rstb.2013.0526

52. Harris RJ, Bookheimer SY, Cloughesy TF, Kim HJ, Pope WB, Lai A, et al. Altered functional connectivity of the default mode network in diffuse gliomas measured with pseudo-resting state fMRI. J Neurooncol. 2014;116: 373–9. doi:10.1007/s11060-013-1304-2

53. Beckmann CF, DeLuca M, Devlin JT, Smith SM. Investigations into resting-state connectivity using independent component analysis. Philos Trans R Soc Lond B Biol Sci.

2005;360: 1001–13. doi:10.1098/rstb.2005.1634

54. Pruim RHR, Mennes M, van Rooij D, Llera A, Buitelaar JK, Beckmann CF. ICA-AROMA: A robust ICA-based strategy for removing motion artifacts from fMRI data. Neuroimage. 2015;112: 267–277. doi:10.1016/j.neuroimage.2015.02.064

55. Jenkinson M, Bannister P, Brady M, Smith S. Improved optimization for the robust and accurate linear registration and motion correction of brain images. Neuroimage. 2002;17: 825–41.

56. Taulu S, Simola J. Spatiotemporal signal space separation method for rejecting nearby interference in MEG measurements. Phys Med Biol. 2006;51: 1759–68. doi:10.1088/0031-9155/51/7/008

57. Hillebrand A, Fazio P, de Munck JC, van Dijk BW. Feasibility of clinical Magnetoencephalography (MEG) functional mapping in the presence of dental artefacts. Clin Neurophysiol. 2013;124: 107–113. doi:10.1016/j.clinph.2012.06.013

58. Hillebrand A, Barnes GR, Bosboom JL, Berendse HW, Stam CJ. Frequency-dependent functional connectivity within resting-state networks: an atlas-based MEG beamformer solution. Neuroimage. 2012;59: 3909–21. doi:10.1016/j.neuroimage.2011.11.005

59. Hillebrand A, Tewarie P, Van Dellen E, Yu M, Carbo EWS, Douw L, et al. Direction of information flow in large-scale resting-state networks is frequency-dependent. Proc Natl Acad Sci U S A. 2016;113. doi:10.1073/pnas.1515657113

60. Douw L, van Dellen E, de Groot M, Heimans JJ, Klein M, Stam CJ, et al. Epilepsy is related to theta band brain connectivity and network topology in brain tumor patients. BMC Neurosci. 2010;11: 103.

61. van Dellen E, Douw L, Heimans JJ, Baayen JC, Ponten SC, Vandertop WP, et al. Long-term effects of temporal lobe epilepsy on local neural networks: a graph theoretical analysis of corticography recordings. PLoS One. 2009;4: e8081.

62. Ruiz-Gómez SJ, Hornero R, Poza J, Maturana-Candelas A, Pinto N, Gómez C. Computational modeling of the effects of EEG volume conduction on functional connectivity metrics. Application to Alzheimer's disease continuum. J Neural Eng. 2019;16: 066019. doi:10.1088/1741-2552/ab4024

63. Stam CJ, Tewarie P, Van Dellen E, van Straaten ECW, Hillebrand A, Van Mieghem P. The trees and the forest: Characterization of complex brain networks with minimum spanning trees. Int J Psychophysiol. 2014;92: 129–138. doi:10.1016/j.ijpsycho.2014.04.001

64. Tewarie P, van Dellen E, Hillebrand A, Stam CJ. The minimum spanning tree: An unbiased method for brain network analysis. Neuroimage. 2015;104: 177–188. doi:10.1016/j.neuroimage.2014.10.015

65. Nissen IA, van Klink NEC, Zijlmans M, Stam CJ, Hillebrand A. Brain areas with epileptic high frequency oscillations are functionally isolated in MEG virtual electrode networks. Clin Neurophysiol. 2016;127: 2581–91. doi:10.1016/j.clinph.2016.04.013

66. Oldham S, Fulcher B, Parkes L, Arnatkeviciūtė A, Suo C, Fornito A. Consistency and differences between centrality measures across distinct classes of networks. PLoS One. Public Library of Science; 2019;14: e0220061. doi:10.1371/journal.pone.0220061

67. Lohmann G, Margulies DS, Horstmann A, Pleger B, Lepsien J, Goldhahn D, et al. Eigenvector centrality mapping for analyzing connectivity patterns in FMRI data of the human brain. PLoS One. 2010;5: e10232.

68. Brookes MJ, Woolrich M, Luckhoo H, Price D, Hale JR, Stephenson MC, et al. Investigating the electrophysiological basis of resting state networks using magnetoencephalography. Proc Natl Acad Sci U S A. 2012;108: 16783–16788.

69. de Pasquale F, Della Penna S, Snyder AZ, Marzetti L, Pizzella V, Romani GL, et al. A cortical core for dynamic integration of functional networks in the resting human brain. Neuron. 2012;74: 753–764.

70. Tang W, Liu H, Douw L, Kramer MA, Eden UT, Hämäläinen MS, et al. Dynamic connectivity modulates local activity in the core regions of the default-mode network. Proc Natl Acad Sci U S A. 2017;114. doi:10.1073/pnas.1702027114

71. Mucha PJ, Richardson T, Macon K, Porter MA, Onnela J-P. Community structure in time-dependent, multiscale, and multiplex networks. Science. 2010;328: 876–8. doi:10.1126/science.1184819

72. Boccaletti S, Bianconi G, Criado R, del Genio CI, Gómez-Gardeñes J, Romance M, et al. The structure and dynamics of multilayer networks. Phys Rep. 2014;544: 1–122. doi:10.1016/j.physrep.2014.07.001

73. Stegehuis C, van der Hofstad R, van Leeuwaarden JSH. Epidemic spreading on complex networks with community structures. Sci Rep. 2016;6: 29748. doi:10.1038/srep29748

74. Cellai D, Dorogovtsev SN, Bianconi G. Message passing theory for percolation models on multiplex networks with link overlap. Phys Rev E. 2016;94: 032301. doi:10.1103/PhysRevE.94.032301

75. Tewarie P, Hillebrand A, van Dijk BW, Stam CJ, O'Neill GC, Van Mieghem P, et al. Integrating cross-frequency and within band functional networks in resting-state MEG: A

multi-layer network approach. Neuroimage. 2016;142: 324–336. doi:10.1016/j.neuroimage.2016.07.057

76. Braun U, Schäfer A, Walter H, Erk S, Romanczuk-Seiferth N, Haddad L, et al. Dynamic reconfiguration of frontal brain networks during executive cognition in humans. Proc Natl Acad Sci U S A. 2015;112: 11678–83. doi:10.1073/pnas.1422487112

77. Mandke K, Meier J, Brookes MJ, O'Dea RD, Van Mieghem P, Stam CJ, et al. Comparing multilayer brain networks between groups: Introducing graph metrics and recommendations. Neuroimage. 2018;166: 371–384. doi:10.1016/j.neuroimage.2017.11.016

78. De Domenico M, Porter MA, Arenas A. MuxViz: a tool for multilayer analysis and visualization of networks. J Complex Networks. Narnia; 2015;3: 159–176. doi:10.1093/comnet/cnu038

79. Rubinov M, Sporns O. Complex network measures of brain connectivity: Uses and interpretations. Neuroimage. 2010;52: 1059–1069.

80. Wechsler D. The Wechsler memory scale-fourth edition (WMS-IV). San Antonio, TX: Pearson Instruments; 2009.

81. van der Elst W, van Boxtel M, van Breukelen G, Jolles J. Rey's verbal learning test: Normative data for 1855 healthy participants aged 24–81 years and the influence of age, sex, education, and mode of presentation. J Int Neuropsychol Soc. Cambridge University Press; 2005;11: 290–302. doi:10.1017/S1355617705050344

82. Schafer JL. Multiple imputation: a primer. Stat Methods Med Res. SAGE Publications; 1999;8: 3–15. doi:10.1177/096228029900800102